

Determination of the mean inner potential of cadmium telluride via electron holography

C. Cassidy, A. Dhar, and T. Shintake

Citation: *Appl. Phys. Lett.* **110**, 163503 (2017);

View online: <https://doi.org/10.1063/1.4981809>

View Table of Contents: <http://aip.scitation.org/toc/apl/110/16>

Published by the [American Institute of Physics](#)

Articles you may be interested in

[Probing the surface potential of oxidized silicon by assessing terahertz emission](#)

Applied Physics Letters **110**, 163502 (2017); 10.1063/1.4980847

[Spontaneously formed high-performance charge-transport layers of organic single-crystal semiconductors on precisely synthesized insulating polymers](#)

Applied Physics Letters **110**, 163302 (2017); 10.1063/1.4981774

[Emergence of a weak topological insulator from the \$\text{Bi}_x\text{Se}_y\$ family](#)

Applied Physics Letters **110**, 162102 (2017); 10.1063/1.4981875

[Surface-enhanced fluorescence in metal nanoparticle-doped polymer nanofibers via waveguiding excitation](#)

Applied Physics Letters **110**, 163101 (2017); 10.1063/1.4981249

[Alloy composition fluctuations and percolation in semiconductor alloy quantum wells](#)

Applied Physics Letters **110**, 162103 (2017); 10.1063/1.4980089

[The absence of ferroelectricity and the origin of depolarization currents in \$\text{YFe}_{0.8}\text{Mn}_{0.2}\text{O}_3\$](#)

Applied Physics Letters **110**, 162905 (2017); 10.1063/1.4981806

Scilight

Sharp, quick summaries **illuminating**
the latest physics research

Sign up for **FREE!**



Determination of the mean inner potential of cadmium telluride via electron holography

C. Cassidy, A. Dhar, and T. Shintake

Quantum Wave Microscopy Unit, Okinawa Institute of Science & Technology Graduate University,
1919-1 Tancha, Onna-son, Okinawa 904-0495, Japan

(Received 3 February 2017; accepted 4 April 2017; published online 19 April 2017)

Mean inner potential is a fundamental material parameter in solid state physics and electron microscopy and has been experimentally measured in CdTe, a technologically important semiconductor. As a first step, the inelastic mean free path for electron scattering in CdTe was determined, using electron energy loss spectroscopy, to enable precise thickness mapping of thin CdTe lamellae. The obtained value was $\lambda_{i(\text{CdTe}, 300\text{ kV})} = 192 \pm 10$ nm. This value is relatively large, given the high density of the material, and is discussed in the text. Next, electron diffraction and specimen tilting were employed to identify weakly diffracting lattice orientations, to enable the straightforward measurement of the electron phase shift. Finally, electron holography was utilized to quantitatively map the phase shift experienced by electron waves passing through a CdTe crystal, with several different propagation vectors. Utilization of both thickness and phase data allowed computation of mean inner potential as $V_{0(\text{CdTe})} = 14.0 \pm 0.9$ V, within the range of previous theoretical estimates. © 2017 Author(s). All article content, except where otherwise noted, is licensed under a Creative Commons Attribution (CC BY) license (<http://creativecommons.org/licenses/by/4.0/>). [<http://dx.doi.org/10.1063/1.4981809>]

CdTe is a II-VI compound semiconductor material, with attractive properties for a number of energy¹ and imaging applications.² These properties include a direct bandgap in the infrared region (1.5 eV), and a relatively high density of 5.85 g/cm³ (which confers enhanced stopping power for high energy radiation).² At present, CdTe is being intensively researched as a direct detector material for tomographic medical imaging,³ but to date it has not seen mainstream application.² Growth of CdTe single crystals is a difficult and expensive process, and present devices are affected by relatively high defect densities and performance instability.² Metal-semiconductor junction formation also plays a critical role in achieving usable devices, particularly the formation of a high-quality Schottky contact to suppress leakage.⁴ To underpin the technological development of CdTe, deeper understanding of both its intrinsic properties, as well as the impact of defects and device processing, is highly desirable. Determination of the mean inner potential is important in both respects.

The mean inner potential, V_0 , is a volumetric average of the electrostatic potential in a solid-state material. It arises from opposing electric field contributions of positive atomic nuclei in the material, and partial screening by dispersed electron clouds, and is thus always a net positive potential. The mean inner potential may be formulated generally as⁵

$$V_0 = \frac{1}{\Omega} \int_{\Omega} V(\vec{r}) d\vec{r}, \quad (1)$$

where Ω is the volume of the unit cell and $V(\vec{r})$ is the variation of electrostatic potential, as a function of position inside the crystal. $V(\vec{r})$ is, in general, not known, being strongly influenced by redistribution of the outer electrons caused by atomic bonding in the solid state.⁵ Determination of the mean inner potential can thus provide insight into bonding

processes that dominate material properties, such as valence electron densities, directionality of covalent bonding, and ionic charge transfer.⁶

Experimentally, the mean inner potential plays a direct role in propagation of electron waves through matter and is thus of central importance for electron diffraction and electron holography. In the absence of magnetic and dynamical diffraction contributions, the phase shift $\Delta\phi$ experienced by an electron wave on passing through a solid specimen with the mean inner potential V_0 can be expressed as⁶

$$\Delta\phi(x, y) = C_E [V_0 + V_{ext}(x, y)] t(x, y), \quad (2)$$

where C_E is a known constant and $t(x, y)$ refers to the specimen thickness. $V_{ext}(x, y)$ describes the contribution of any additional electric fields (arising, for example, from residual charge, engineered semiconductor junctions, or applied external bias). The phase shift $\Delta\phi(x, y)$ can be quantitatively mapped with high resolution by electron holography. Assuming that $t(x, y)$ can be determined by independent methods, Eq. (2) allows direct mapping of the internal potential distributions within a material. In the first instance, in the absence of external potentials, electron holography can be utilized to determine V_0 (the subject of the current work). Furthermore, once the mean inner potential is known, more advanced studies can proceed to analyze the fields associated with extrinsic nanoscale features, such as patterned electrical junctions⁷ or crystallographic defects.⁸

For execution of experiments, unprocessed single crystal CdTe samples were obtained from Acrorad, Ltd. (Okinawa, Japan).⁹ Electron transparent samples were prepared using an FEI Helios 650 Nanolab Focused Ion Beam (FIB) system. Electron Energy Loss Spectroscopy (EELS) and holography experiments were performed using an FEI Titan transmission

electron microscope, operated at 300 kV. Electron Energy Loss Spectroscopy (EELS) data were acquired in STEM mode, utilizing a post-column Gatan Quantum 966. Holography data acquisition employed a Lorentz mini-lens and an electrostatic biprism mounted in the selected area aperture plane (off-axis configuration⁶). Full experimental details are included in the [supplementary material](#).

As mentioned briefly, specimen thickness must be determined independently. EELS is particularly suited to the task of mapping specimen thickness with high precision,¹⁰ but the absolute thickness measurement requires knowledge of the inelastic scattering probabilities, embodied by the mean free path, λ_i . Therefore, an initial sequence of experiments was performed to determine the inelastic mean free path of CdTe at an accelerating voltage of 300 kV, thereby enabling calibrated EELS thickness mapping for subsequent mean inner potential calculation.

Specimens with well-defined geometries were prepared using FIB and analyzed using EELS. In Figure 1(a), one can see a plan view SEM image, illustrating the geometry of the sample after FIB milling (in this case, a 15° wedge sample). In Figure 1(b), one can see a side-view TEM image of the same specimen, in which the protective capping layers and the contrast variation associated with the wedge thickness can be observed. In Figure 1(c), a STEM image is shown, with Label “SI” indicating a spectrum image region from which an EELS spectrum was acquired at each pixel. A typical low-loss EELS spectrum from CdTe is shown in Figure 1(d). It is evident that CdTe exhibits a rather broad plasmon feature centered at approximately 14 eV energy loss, as well as a relatively large background, arising from the excitation of single outer shell electrons.¹⁰ The details of the energy loss spectrum are not the focus of the current work, but rather that the relative quantities of loss (inelastically scattered) and zero-loss (elastically scattered) electrons allow the relative specimen thickness, t/λ_i , to be determined. In this context, I_T (blue) refers to the total integrated counts from electrons that passed through the specimen and were detected by the spectrometer. I_{ZL} refers to the integrated counts in the zero-loss peak (which

is determined by fitting the I_T data using a pre-acquired vacuum reference). The relative thickness, t/λ_i , can be computed according to the equation shown in Fig. 1(d).¹⁰ It is worth pointing out that the spectrometer collection (or acceptance) angle can directly affect the EELS thickness measurement in the small collection angle regime, before reaching a stable value at larger angles.¹² With this in mind, we performed supporting experiments to calibrate the collection angle and to explore the effect of the collection angle on the EELS measurement. As expected, in the large angle regime, the EELS data showed no significant dependence on the collection angle (see Fig. S3, [supplementary material](#), for example), and thus, the maximum available collection angle of 40.5 mrad was utilized for all subsequent measurements.

A map of relative thickness can be created by processing spectra in each pixel of region “SI,” as shown in Fig. 1(e). The t/λ_i values vary in a linear fashion with specimen thickness, as shown in Fig. 1(f), which shows a line profile extracted along QQ'. No problems with linearity were evident in the thin region (where surface plasmon effects might contribute strongly¹⁰) or in the thick region (where multiple scattering may cause non-linear behavior¹¹). These data confirm the validity of EELS measurements of CdTe thickness in this range. As this method relies on prior knowledge of the specimen geometry, and real milled samples may deviate slightly from the intended mathematical design, seven samples with different thicknesses and geometries were made to improve the measurement quality. Figure 2 shows the aggregation of the EELS data from these seven samples. The linearity and mutual agreement, from samples with markedly different thicknesses and ion-milling geometries, are quite good. This EELS dataset, in conjunction with known specimen thickness, leads to a mean value for $\lambda_{i(\text{CdTe}, 300\text{ kV})}$ of 192 nm, with a standard deviation of 10 nm. This value is required in the current work to enable calibrated thickness mapping but is also of great benefit for other electron-beam techniques, such as quantitative EELS for compositional or bonding studies. The relatively large CdTe value is also advantageous for those techniques that require a single-

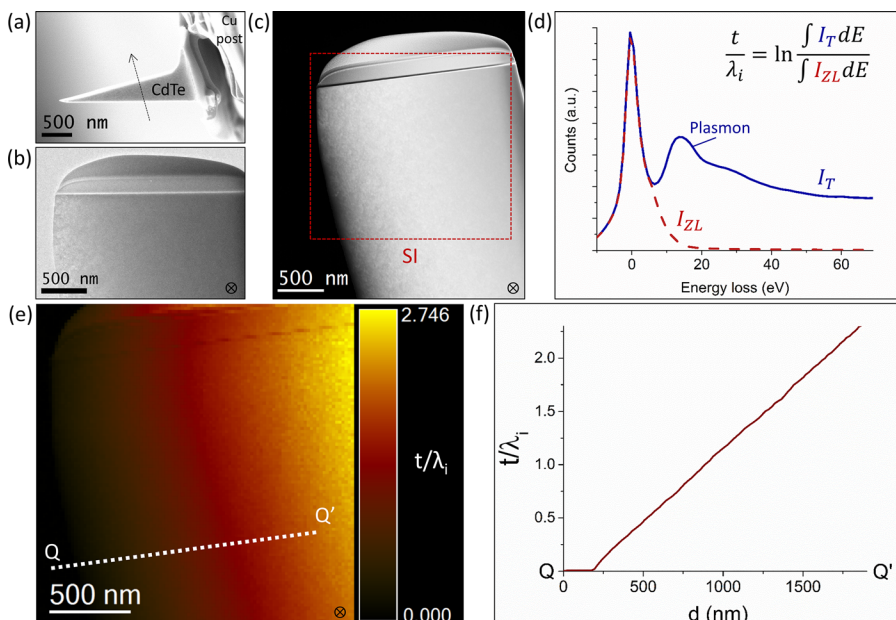


FIG. 1. Methodology of EELS measurements of λ_i . (a) Plan view SEM image after ion milling, showing a sample with a defined 15° wedge. (b) Low-magnification side view TEM view of the wedge sample. (c) STEM image and highlighted area for 2D EELS mapping, labeled “SI.” (d) Example raw EELS spectrum, I_T , and fitted zero-loss peak, I_{ZL} , used to calculate t/λ_i ; (e) 2D map of t/λ_i , from region “SI” in (c), generated using the ratio of loss and zero-loss EELS counts. (f) Example profile, extracted along Q-Q’ in (e), demonstrating the uniformity, linearity, and apex sharpness of this wedge sample. Such t/λ_i data, in conjunction with prior knowledge of the specimen thickness and geometry, allow λ_i to be determined. Note that the direction of the electron beam in TEM is indicated by the dotted arrow in (a) and the \otimes symbol in (b)–(e).

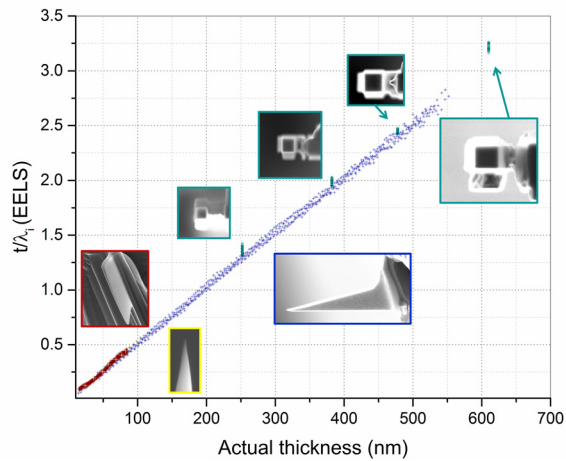


FIG. 2. Measurement of $(t/\lambda_i)_{\text{CdTe}}$, as a function of milled specimen thickness. The measured t/λ_i values varied in a quite linear fashion with milled specimen thickness, across multiple samples with different dimensions and geometries. In aggregate, these data yield $\lambda_{i(\text{CdTe}, 300\text{ kV})}$ mean and standard deviation of 192 nm and 10 nm, respectively.

scattering distribution ($t/\lambda < 0.3$), in that reasonably thick samples can be investigated.

For comparison purposes, the mean free path for silicon (with much lower density and atomic number) has been previously reported to be 180–200 nm, via EELS.^{11,12} Additionally, Gan *et al.* recently measured the mean free path of ZnTe (a rather similar material to CdTe) to be 46 nm (Ref. 13) via holography amplitude measurements. Therefore, to place the CdTe value in a wider context, it is important to clarify the definition of mean free path, and the electron scattering processes that underpin it. In the current work, the EELS spectrometer did not resolve any energy loss events below 5 eV, so small energy losses, such as those associated with phonon excitations, were not detected. The majority of detected energy loss events were then primarily plasmon excitations and single-electron transitions.¹⁰ The scattering probabilities for these events depend on, in a very complex way, the electronic band structure of the material,¹⁴ and it is not unexpected that CdTe, despite being a high-Z material, will exhibit a relatively long mean free path. Holography measurements of mean free path, on the other hand, are sensitive to even very low energy loss events (such as phonon scattering), given the stringent coherency requirements for interference to occur.⁶ Furthermore, blocking of elastically scattered electrons by system apertures (scattering absorption) is an important consideration for holographic measurements of mean free paths. The theoretical background and pertinent experimental considerations have been explained in detail.^{20,21} The ZnTe measurements by Gan *et al.*¹³ utilized a very small aperture of 0.75 mrad, presumably resulting in significant scattering absorption. Considering both of these effects, it is therefore logical that the holographic measurements of mean free path, as reported by Gan *et al.* for ZnTe, are much shorter. A key point is that in considering mean free path for electron scattering, caution must be exercised regarding the types of scattering event, or energy range, that contribute to the measurement.

As the next step involves phase measurements, the topic of dynamical diffraction must be introduced. Dynamical diffraction refers to repeated electron wave scattering upon

propagation through a crystal. It directly affects wave amplitude and phase and is particularly pronounced in single crystalline materials oriented close to a Bragg condition.¹⁵ It is a complex phenomenon, which can cause very significant electron wave phase shifts that vary dramatically with only slight lattice orientation or thickness changes.¹³ It has been studied systematically by Lubk *et al.*,²² who explored the effect of dynamical diffraction on the mean inner potential measurements, as a function of simulation methodology, microscope parameters and specimen thickness, orientation, and composition. They found that dynamical scattering results in a systematic underestimation of the mean inner potential, and that the dynamical contribution was reduced as a function of tilt away from low-index crystallographic zone axes. Therefore, for CdTe experimental measurements, a brief study was conducted to ensure that such dynamical contributions were minimized (Fig. 3). The tilt angles of three primary poles ([100], [110], and [111]), and numerous weakly diffracting orientations, were identified using converged beam electron diffraction (CBED), on a CdTe needle sample. Electron holograms were also acquired at each tilt angle according to the usual off-axis scheme (further details on acquisition, reconstruction, and sign conventions are included in the [supplementary material](#)). In Fig. 3(a), one can see the CBED patterns acquired at each tilt angle, while in Figure 3(b), the locations of each acquisition are indicated on a stereographic projection (exact tilt angles are tabulated in Table S1, [supplementary material](#)). In Figure 3(c), the impact of dynamical diffraction on the phase value is illustrated. Line profiles have been extracted from the phase images, along the long axis of the needle, at each of the tilt angles. When oriented to a low-index zone axis (red), one can see that the measured phase shows very large changes with the position, which is consistent with strong dynamical diffraction effects. When the crystal is tilted away from low-index zone axes (blue), however, one can see that the phase value changes in a stable and monotonic fashion with thickness, which is a confirmation that dynamical diffraction effects are not contributing significantly. Thus, it can be concluded that the phase data collected at these tilt angles (A-E) may be safely used in Equation (2) for computation of the mean inner potential.

This computation of the mean inner potential requires both thickness and phase data, and a practical issue concerns the different pixel sizes, dimensions, and orientations of the images produced by the rastered STEM-EELS (Fig. 4(a)) and optical Lorentz-holography (Fig. 4(b)). With this in mind, a short Matlab code was written to resample and align the thickness and phase 2D data arrays and to perform the computation (details in the [supplementary material](#)). The computed mean value for the mean inner potential was 14.0 V, with a standard deviation of 0.9 V (Fig. 4(c)).

Several theoretical estimates of the mean inner potential of CdTe have been reported previously. Schowalter *et al.*¹⁶ performed *ab initio* calculations of V_0 in CdTe, utilizing density functional theory (DFT), and obtained values of 13.61 V and 13.67 V (depending on the exact DFT formalism used). This methodology had already been experimentally verified for some other materials (GaAs, ZnTe¹³) and also seems to work well for CdTe. Several analytical calculations have also been reported, based upon the atomic Cd and Te reference

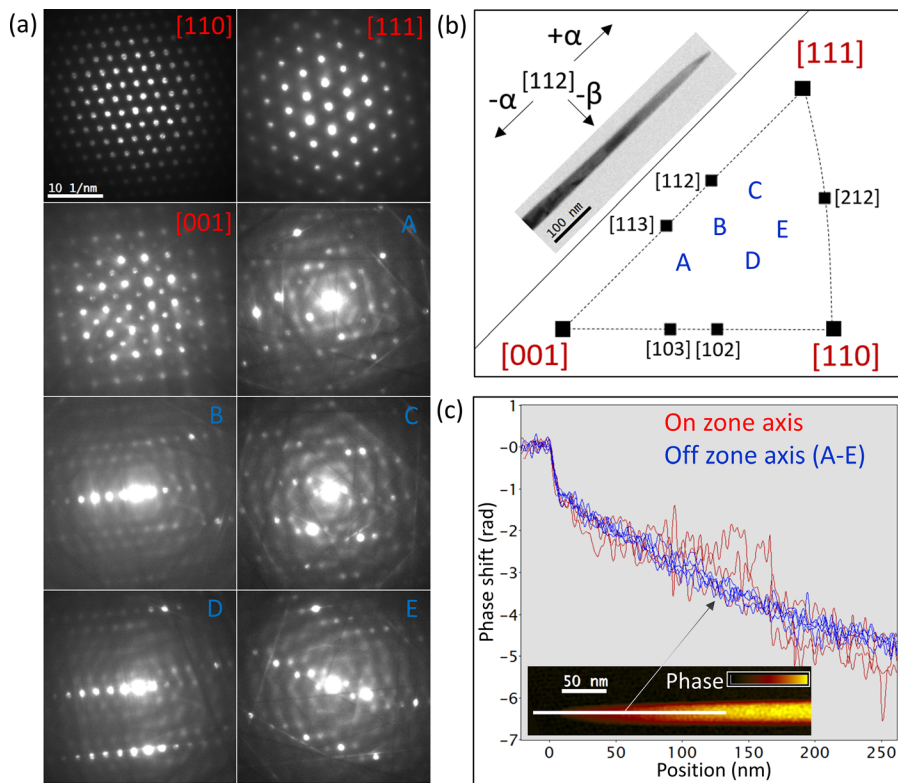


FIG. 3. Identification of crystal tilt angles *without* significant dynamical diffraction contributions. (a) CBED patterns as a function of specimen tilt (exact angles are tabulated in Table S1, [supplementary material](#)). Inset: atomic models of the associated crystal orientation (red: Cd; yellow: Te atoms). (b) illustration of the TEM holder α and β tilt directions with respect to the CdTe needle axis, and stereographic projection of the tilt region examined, showing the principal poles as well as locations of off-zone-axis hologram acquisition. (c) Overlaid phase profiles from the CdTe specimen as a function of position on the needle for different specimen tilts. Each of these 1D profiles, along the needle long axis, was extracted from the corresponding 2D phase image, as illustrated in the inset. It is clear that phase data acquired from low index zone axes (red) are affected by erratic dynamical contributions, while off-axes phase data (blue) varies monotonically with specimen thickness.

data from the literature and by applying approximations to deal with electron redistribution when atoms are bonded in a crystalline lattice. Dvoryankina *et al.*¹⁷ performed calculations which utilized published values for Cd and Te mean square atomic radii as the starting point, and assumed that electron redistribution effects can be ignored for mean inner potential calculations for covalently bonded materials. They obtained a value of 14.765 V for CdTe. This is somewhat higher than the DFT value¹⁶ but is still well within the experimental distribution. Another established methodology⁵ involves (i) utilizing Doyle-Turner atomic scattering factors; (ii) estimating an upper limit by assuming that the lattice is composed of distinct, non-bonded, neutral atoms (the “isolated atom” or “non-binding” approximation); and (iii) estimating a lower limit by applying an empirically derived correction factor (the “Ross-Stobbs” approximation). Applying this methodology to CdTe, in the same fashion as for ZnTe,¹³ yields an upper value of 14.2 V and a lower value of 10.3 V. The experimental value certainly falls within this range, but it is clear that the experimental distribution is centered very close

to the non-binding value. This lends weight to the assumption that the non-binding approximation yields accurate values for covalently bonded materials.¹⁷

The standard deviation of 0.9 V in the experimental data, while considered acceptable for this Letter announcing first measurements of this parameter, should be further reduced by conducting a more detailed study and by addressing a number of specific issues. In particular, the contribution from the specimen surface (lattice orientation, oxidation state, and adsorbed species) warrants a dedicated study.^{18,19} A more systematic study of the contributions of dynamical diffraction would also be beneficial.^{13,22} The roles of synthesis method, crystal quality, and trace impurities should also be investigated. Measurements could also be acquired at multiple accelerating voltages, temperatures, electron dose rates, and specimens with different specimen geometries, to obtain a fuller picture of the mean inner potential for this semiconductor material.

In conclusion, we have applied electron energy loss spectroscopy, converged beam electron diffraction, and off-

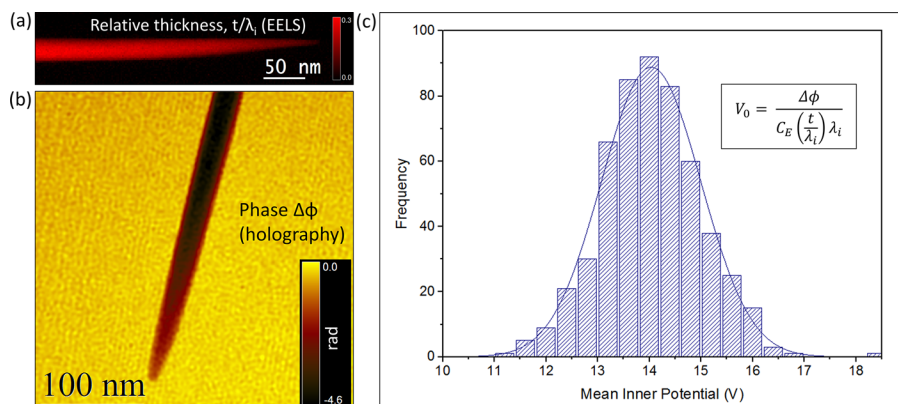


FIG. 4. Computation of the mean inner potential of CdTe. (a) Thickness map, obtained with STEM-EELS, (b) phase map, obtained using off-axis holography and numerical reconstruction, and (c) the mean inner potential values, computed from the thickness and phase arrays, according to the equation shown in the inset.

axis electron holography to obtain values for the EELS mean free path λ_i (at 300 kV) and the mean inner potential, V_0 , of CdTe. The obtained values provide basic insights into the electronic structure of the material and should be useful for those engaged in simulation or microscopy studies of this material. CdTe shows significant promise for energy and imaging applications, and the reported values will facilitate efforts to further understand and develop this material.

See [supplementary material](#) for additional experimental details, holography data, and tabulated specimen tilt angles.

The provision of CdTe specimens by AcroRad, Ltd., and by Dr. Shin'ichiro Takeda (OIST) is gratefully acknowledged. The authors would also like to thank Dr. Steven Aird for useful discussions and editing the manuscript.

- ¹J. M. Burst, J. N. Duenow, D. S. Albin, E. Colegrove, M. O. Reese, J. A. Aguiar, C.-S. Jiang, M. K. Patel, M. M. Al-Jassim, D. Kuciauskas, S. Swain, T. Ablekim, K. G. Lynn, and W. K. Metzger, *Nat. Energy* **1**, 16015 (2016).
- ²J. Iwanczyk and K. Iniewski, *Radiation Detectors for Medical Imaging* (CRC Press, 2016).
- ³Z. Yu, S. Leng, S. Kappler, K. Hahn, Z. Li, A. F. Halaweish, A. Henning, and C. H. McCollough, *J. Medical Imaging* **3**(4), 043503 (2016).
- ⁴T. Takahashi, T. Mitani, Y. Kobayashi, M. Kouda, G. Sato, S. Watanabe, K. Nakazawa, Y. Okada, M. Funaki, R. Ohno, and K. Mori, *IEEE Trans. Nucl. Sci.* **49**, 1297 (2002).
- ⁵M. Gajdardziska-Josifiska and A. H. Carim, "Introduction to Electron Holography," in *Applications of Electron Holography* edited by E. Voelkl, L. F. Allard, and D. Joy (Springer Science, 1999), Chap. 12.
- ⁶H. Lichte and M. Lehmann, *Rep. Prog. Phys.* **71**, 016102 (2008).
- ⁷A. C. Twitchett, R. E. Dunin-Borkowski, and P. A. Midgley, *Phys. Rev. Lett.* **88**, 238302 (2002).
- ⁸D. Cherns and C. G. Jiao, *Phys. Rev. Lett.* **87**, 205504 (2001).
- ⁹M. Ohmori, Y. Iwase, and R. Ohno, *Mater. Sci. Eng., B* **16**, 283–290 (1993).
- ¹⁰R. F. Egerton, *Electron Energy Loss Spectroscopy in the Electron Microscope*, 3rd Ed. (Springer, 2011).
- ¹¹H. Meltzman, Y. Kauffmann, P. Thangadurai, M. Drozdov, M. Baram, D. Brandon, and W. D. Kaplan, *J. Microsc.* **236**, 165–173 (2009).
- ¹²C.-W. Lee, Y. Ikematsu, and D. Shindo, *J. Electron Microsc.* **51**(3), 143–148 (2002).
- ¹³Z. Gan, M. DiNezza, Y.-H. Zhang, D. J. Smith, and M. R. McCartney, *Microsc. Microanal.* **21**, 1406–1412 (2015).
- ¹⁴K. Iakoubovskii and K. Mitsuishi, *Phys. Rev. B* **77**, 104102 (2008).
- ¹⁵D. B. Williams and C. B. Carter, *Transmission Electron Microscopy*, 2nd ed. (Springer, 2009).
- ¹⁶M. Schowalter, D. Lamoen, A. Rosenauer, P. Kruse, and D. Gerthsen, *Appl. Phys. Lett.* **85**, 4938 (2004).
- ¹⁷G. G. Dvoryankina, V. F. Dvoryankina, and A. G. Petrov, *Crystallography Rep.* **53**(2), 187–191 (2008).
- ¹⁸D. K. Saldin and J. C. H. Spence, *Ultramicroscopy* **55**, 397–406 (1994).
- ¹⁹R. S. Pennington, J. J. Mortensen, T. Kasama, C. B. Boothroyd, and R. E. Dunin-Borkowski, *J. Phys.: Conf. Ser.* **209**, 012030 (2010).
- ²⁰F. Kern, D. Wolf, P. Pschera, and A. Lubk, *Ultramicroscopy* **171**, 26–33 (2016).
- ²¹A. Lubk, D. Wolf, F. Kern, F. Röder, P. Prete, N. Lovergine, and H. Lichte, *Appl. Phys. Lett.* **105**, 173101 (2014).
- ²²A. Lubk, D. Wolf, and H. Lichte, *Ultramicroscopy* **110**, 438–446 (2010).